Formation of Giant Spicule from Quartz Glass by the Deep Sea Sponge *Monorhaphis*

Werner E. G. Müller,*,† Klaus Peter Jochum,*,‡ Brigitte Stoll,‡ and Xiaohong Wang§

Institut für Physiologische Chemie, Abteilung Angewandte Molekularbiologie, Universität Mainz, Duesbergweg 6, D-55099 Mainz, Germany, Max-Planck-Institut für Chemie, J.J. Becherweg 27, D-55128 Mainz, Germany, and National Research Center for Geoanalysis, 26 Baiwanzhuang Dajie, CHN-100037 Beijing, P.R. China

Received March 12, 2008. Revised Manuscript Received April 24, 2008

The skeleton of the oldest multicellular animals, the spicules from siliceous sponges (the classes of Hexactinellida and Demospongiae), is composed of amorphous hydrated silica. The most outstanding feature of these spicules is that they are synthesized by the enzyme silicatein. After having studied the largest biosilica structures on earth, the up to 3 m long (diameter of 8.5 mm) spicules from the deep-sea hexactinellid *Monorhaphis chuni*, we describe that this silica material has the quality of quartz glass. Although such silica can be produced chemically only at high temperature and with aggressive chemicals, the animals fabricate this biomaterial physiologically and at low temperature (around 4 °C). These giant spicules are composed of almost pure silica. Likewise surprising is the fact that this biosilica contains a proteinaceous matrix, which is silicatein. Because these composite structured spicules also function as excellent light waveguides, our results may open new perspectives for the production of nanostructured materials and devices in the opto- and microelectronics industry.

Introduction

Sponges [Phylum Porifera] are simple and the evolutionary oldest animals that appeared approximately 800−600 million years ago, as the first metazoans on our planet.[1–3] This important phylum remained enigmatic for a long time. However, during the last 12 years, our studies, mainly by application of molecular biological and cell biological techniques, revealed that sponges share most features with other metazoans, such as the cell communication and adhesion systems,[4] the immune system,[5] the mechanisms of apoptotis, or the body plan.[6] These characteristics qualify the sponges as the basal taxon of all metazoan phyla, which allows exploring the "common roots" of all animals.[7] Nevertheless, sponges are distinguished by one unique feature from all other metazoans: they synthesize their siliceous skeleton enzymatically by silicatein.[8–11] These amazing results were obtained with siliceous sponges, which are grouped into the classes of Demospongiae and Hexactinellida. Recently, first evidence has been presented that silica formation might require collagen[12] and/or chitin.[13] Major progress had been achieved with the discovery that Demospongiae, with the species *Tethya aurantium*[8,9] and *Suberites domuncula*[10] as models, have the unique property of being able to synthesize their skeleton [spicules] of amorphous biosilica, enzymatically at the body temperature of the animals.[11] A boost toward a practical application of sponge biosilica came from studies of Aizenberg et al.[14] and us,[15] which revealed that spicules, especially from hexactinellids, can be used as optical fibers with exceptional properties. For those studies, some relatively small spicules from *Euplectella aspergillum* or *Hyalonema sieboldi*, with lengths of 5−8 cm (fragments) and diameters of <0.5 mm, had been used. These

* To whom correspondence should be addressed. E-mail: wmueller@uni-mainz.de (W.E.G.M.); kpj@mpch-mainz.mpg.de (K.P.J.). Tel.: 49-6131-39 25910 (W.E.G.M.); 49-6131-305 216 (K.P.J.). Fax: 49-6131-39 25243 (W.E.G.M.); 49-6131-371 051 (K.P.J.). Web site: http://www.biotecmarin.de/ (W.E.G.M.).
† Universität Mainz.
‡ Max-Planck-Institut für Chemie.
§ National Research Center for Geoanalysis.

(1) Müller, W. E. G.; Wiens, M.; Adell, T.; Gamulin, V.; Schröder, H. C.; Müller, I. M. *Int. Rev. Cytol.* **2004**, *235*, 53–92.
(2) Schäcke, H.; Müller; I. M.; Müller, W. E. G. In *Use of Aquatic Invertebrates as Tools for Monitoring of Environmental Hazards*; Müller, W. E. G., Ed.; Gustav Fischer Verlag: Stuttgart, Germany, 1994; pp. 201−211.
(3) Brasier, M. D.; Green, O.; Shields, G. *Geology* **1997**, *25*, 303–306.
(4) Pancer, Z.; Kruse, M.; Schäcke, H.; Scheffer, U.; Steffen, R.; Kovács, P.; Müller, W. E. G. *Cell Adhes. Commun.* **1996**, *4*, 327–339.
(5) Müller, W. E. G.; Blumbach, B.; Müller, I. M. *Transplantation* **1999**, *68*, 1215–1227.
(6) Müller, W. E. G. Spatial and temporal expression patterns in animals. In *Encyclopedia of Molecular Cell Biology and Molecular Medicine*; Meyers, R. A., Ed.; Wiley-VCH Press: Weinheim, Germany, 2005; Vol. 13, pp 269−309.
(7) Pilcher, H. *Nature* **2005**, *435*, 1022–1023.
(8) Shimizu, K.; Cha, J.; Stucky, G. D.; Morse, D. E. *Proc. Natl. Acad. Sci. U.S.A.* **1998**, *95*, 6234–6238.
(9) Cha, J. N.; Shimizu, K.; Zhou, Y.; Christianssen, S. C.; Chmelka, B. F.; Stuck, G. D.; Morse, D. E. *Proc. Natl. Acad. Sci. U.S.A.* **1999**, *96*, 361–365.
(10) Krasko, A.; Batel, R.; Schröder, H. C.; Müller, I. M.; Müller, W. E. G. *Eur. J. Biochem.* **2000**, *267*, 4878–4887.
(11) Müller, W. E. G.; Schlossmacher, U.; Wang, X.; Boreiko, A.; Brandt, D.; Wolf, S. E.; Tremel, W.; Schröder, H. C. *FEBS J.* **2008**, *275*, 362–370.
(12) Ehrlich, H.; Heinemann, S.; Heinemann, C.; Simon, P.; Bazhenov, V. V.; Shapkin, N. P.; Born, R.; Tabachnick, K. R.; Hanke, T.; Worch, H. J. *Nanomaterials* **2008**, doi:10.1155/2008/623838, in press.
(13) Ehrlich, H.; Maldonado, M.; Spindler, K. D.; Eckert, C.; Hanke, T.; Born, R.; Goebel, C.; Simon, P.; Heinemann, S.; Worch, H. *J. Exp. Zool.* **2007**, *308B*, 347–356.
(14) Aizenberg, J.; Sundar, V. C.; Yablon, A. D.; Weaver, J. C.; Chen, G. *Proc. Natl. Acad. Sci. U.S.A.* **2004**, *101*, 3358–3363.
(15) Müller, W. E. G.; Wendt, K.; Geppert, C.; Wiens, M.; Reiber, A.; Schröder, H. C. *Biosens. Bioelectron.* **2006**, *21*, 1149–1155.

10.1021/cm800734q CCC: $40.75
Published on Web 06/18/2008

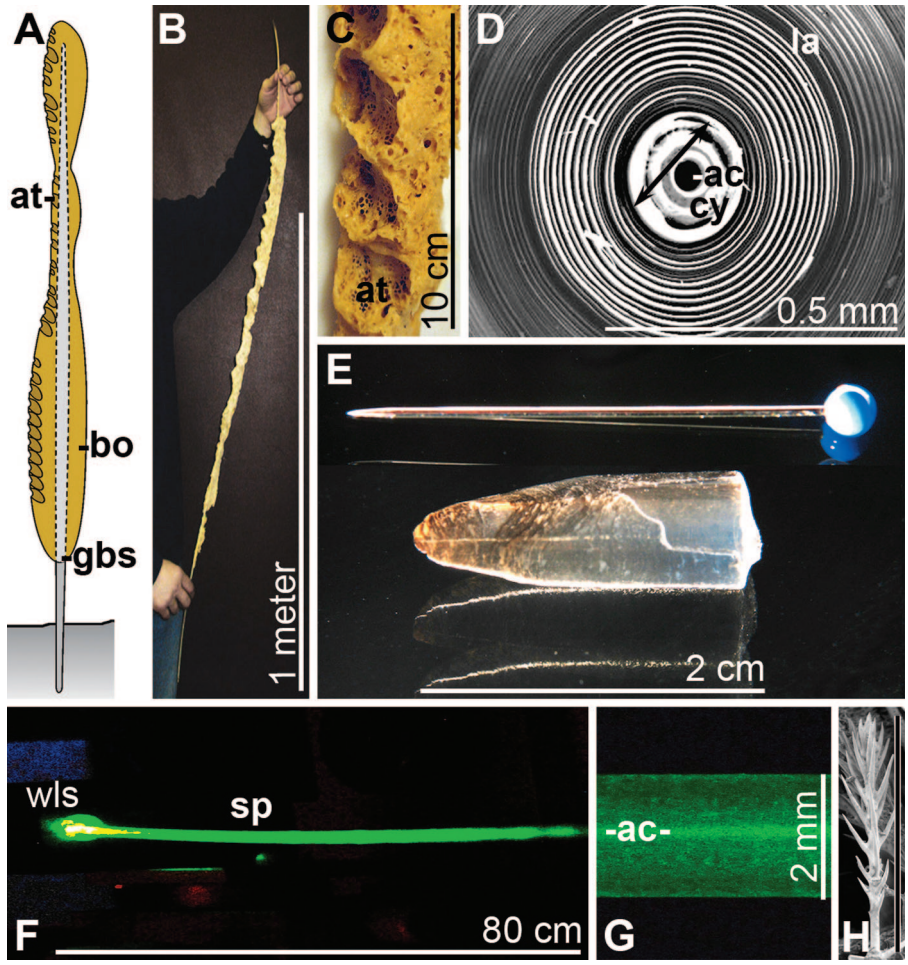

Figure 1. Hexactinellid *Monorhaphis* (*M. chuni*/*M. intermedia*) with its giant basal spicule. (A) Schematic growth pattern of this animal. Small specimens surround the giant basal spicule completely. During growth, the body (bo), displaying one row of atrial openings that harbor the excurrent canals of the aquiferous system, elongates and grows along the centrally arranged giant spicule (gbs) to reach a final size of 3 m. (B) 1 m long spicule, shown being held by a person. The atrial openings are at one side of the animals. (C) A series of atrial openings (at). (D) Polished cross section through a giant basal spicule, displaying its three parts (i) the axial canal (ac), (ii) the axial cylinder (cy) and (iii) the lamellar region (la). (E) Comparison between the tip of a giant basal spicule (diameter of 7 mm) and a pin/needle. (F) A white light source (wls) focused onto one end of the monaxial giant basal spicule (sp), showing the transmission of light within the spicule. (G) Higher magnification of the illuminated spicule, uncovering the axial canal (ac), which appears brighter because of the higher reflection. (H) Comparatively small spicules stabilize the body of the animal; among the 10 different types of spicules is the pinular pentactine that is shown. Length of this spicule (bar): 20 μm.

hexactinellid spicules had been described to be constructed hierarchically from nanometer-sized building blocks, and to grow by apposition of lamellae.[16,17]

To better understand the structure of the hexactinellid spicules, our group has introduced the giant basal spicules from *Monorhaphis chuni*/*Monorhaphis intermedia* [(perhaps) synonymic species] (Porifera: Hexactinellida: Amphidiscosida: Monorhaphididae) as model. Specimens of this species form one giant spicule each, the giant basal spicule, which can reach lengths of 3 m and diameters up to 8.5 mm.[16,18] This size qualifies those silica structures to be exceptionally suitable for morphological and detailed inorganic and organic analytical studies. The first specimens of this giant sponge species were discovered by dredging at a depth of 1600 m, during the Valdivia Expedition off the coast of East Africa (Somalia basin) in 1904 by Schulze.[18] They were also found in the South Chinese Sea and around New Caledonia in the deep pelagic zone.[16,19]

Results and Discussion

Giant Basal Spicules of *Monorhaphis*. The body of one Monorhaphis specimen is organized around one giant basal spicule, earlier termed basalia, as shown schematically in Figure 1A. In addition, ten much smaller spicule types are found in the body, with the relatively tiny 10−70 μm long pinular pentactines as an example (Figure 1H). The osculi, which merge the excurrent canals of the aquiferous system, are arranged in atrial openings that are aligned at the side of the sponge body facing low current (Figure 1A−C). The remaining surface displays the much smaller incurrent canals

(16) Müller, W. E. G.; Eckert, C.; Kropf, K.; Wang, X.; Schlossmacher, U.; Seckert, C.; Wolf, S. E.; Tremel, W.; Schröder, H. C. *Cell Tissue Res.* **2007**, *329*, 363–378.
(17) Weaver, J. C.; Aizenberg, J.; Fantner, G. E.; Kisailus, D.; Woesz, A.; Allen, P.; Fields, K.; Porter, M. J.; Zok, F. W.; Hansma, P. K.; Fratzl, P.; Morse, D. E. *J. Struct. Biol.* **2007**, *158*, 93–106.
(18) Schulze, F. E. *Hexactinellida. Wissenschaftliche Ergebnisse der Deutschen Tiefsee-Expedition auf dem Dampfer "Valdivia" 1898−1899*; Gustav Fischer Verlag: Stuttgart, Germany, 1904; pp 1−266.
(19) Woesz, A.; Weaver, J. C.; Kazanci, M.; Dauphin, Y.; Aizenberg, J.; Morse, D. E.; Fratzl, P. *J. Mater. Res.* **2006**, *21*, 2068–2078.

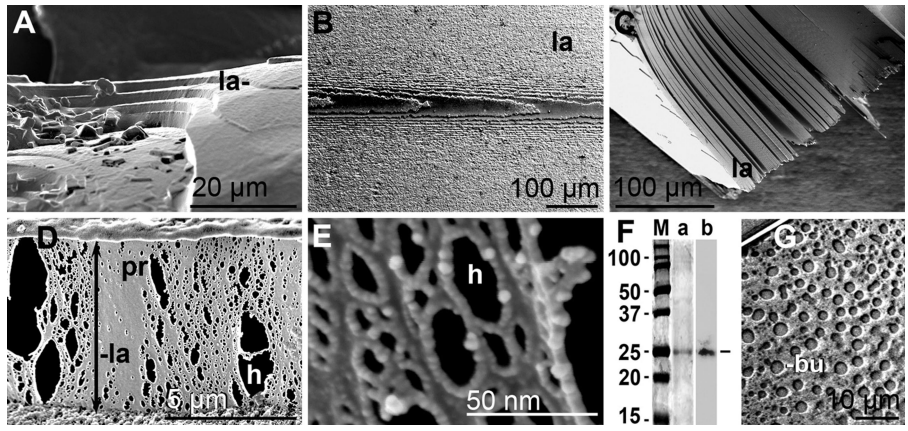

Figure 2. Lamellar organization of the giant basal spicules. (A) Cross fracture through a spicule revealing the stepwise arrangement of the lamellae (la). (B) Longitudinal axial cut disclosing the concentric organization of the lamellae (la). (C) Opening of a pile of the concentric sheets/lamellae (la), after cutting the spicule in axial direction. (D) Etching of the cross-section with HF vapor results in the dissolution of the dense biosilica lamella (la), leaving behind the proteinaceous palisade-like scaffold protein (pr). (E) Higher magnification of this protein construction showing that the fibers are interconnected, leaving open holes (h) whose rims are reinforced by densely arranged 10 nm spheres. (F) Analysis of the protein, existing in the spicules, by NaDodSO4-PAGE. After being stained with Coomassie brilliant blue, one band (25 kDa) becomes visible (lane a, thin line). This 25 kDa band cross-reacts with anti-silicatein antibodies after Western blotting (lane b). In parallel, protein markers were run (M). (G) After heating the spicules to 450 °C, perforation bubbles (bu) on the surfaces are seen that disclose concentric 1 μm large holes.

(Figure 1C). The spicule that we used for the experiments here was about 110 cm long and had a maximum diameter of 7 mm (Figure 1E). Scanning electron microscopic [SEM] inspection of cross-sections through giant basal spicules reveals their lamellar organization. In the center of the spicules is located the axial canal, which harbors the axial filament. This canal is surrounded by the axial cylinder with a diameter of about 100 μm, around which the lamellar zone is concentrically arranged (Figure 1D). The appositional growth of these spicules, lamella upon lamella, has recently been described.[16] Each lamella is 3−7 μm thick (in *Monorhaphis*). Hence, more than 500 lamellae can be counted around the axial cylinder. The axial filament, existing in the axial canal, is formed from self-assembled silicatein molecules as has been demonstrated in *S. domuncula*.[20,21] The monaxonal giant basal spicules from *Monorhaphis* function as optical waveguide (Figure 1F), which transmits, like in *Hyalonema sieboldi*,[15] incident light efficiently between 800 and 1200 nm. The axial canal becomes visible because of the reflection of the light (Figure 1G).

Cross fractures through a giant basal spicule show a stepwise layering of the ~5 μm high silica-lamellae (Figure 2A), reflecting the appositional growth, which is also corroborated by a longitudinal cut (Figure 2B). If the giant basal spicule is sectioned along its axis, the concentrically arranged sheets/lamellae open up and unfold (Figure 2C). This observation supports earlier findings,[19,22] that the contact between the lamellae is not tight, thus allowing an individual breakage of the lamellae. If siliceous spicules are exposed to hydrofluoric acid (HF), the biosilica is dissolved.[23] However, if they are exposed to HF vapor, as shown here with the giant basal spicules, a proteinaceous palisade-like scaffold can be uncovered (Figure 2D). This fibrous structure is interspersed with holes that are formed by the interconnecting fibers. Interestingly, at higher magnification and by using the high-resolution SEM technique, it becomes overt that the rim of each hole is reinforced by densely arranged 10−15 nm large spheres (Figure 2E), as reported.[12,22] The total protein from the lamellar zone of the spicules was obtained by dissolving the biosilica with HF; the residual protein was quantified by the Bradford method[24] and found to account for 4.6% [w/w] of the total weight of the spicules.

Silicatein. The (major) protein existing in the spicules of *Monorhaphis* was analyzed by sodium dodecyl sulfate polyacrylamide gel electrophoresis (NaDodSO4-PAGE). Only one band with a size of 25 kDa could be visualized after staining with Coomassie brilliant blue; and again only this 25 kDa protein reacted with the anti-silicatein antibodies raised against the *S. domuncula* protein (Figure 2F, lanes a and b).[20] This result can be taken as a first indication that silicatein is the major protein in the spicules in hexactinellids as well. This assumption can be supported by deducing/calculating from the size of the 10−15 nm spheres visualized by SEM, to the size of the molecule(s). In reference to human serum albumin with a size of 65 kDa and a dimension of 3− 8 nm,[25] the 10−15 nm spheres framing the holes of the proteinaceous scaffold within a silica lamella would correspond to a size of 130 kDa. This figure corresponds to approximately five silicatein molecules, a number that had been experimentally shown to assemble if native samples from *S. domuncula* are analyzed.[21,26] In addition to the organic components and inorganic minerals, the sponge biosilica also contains water.[27,28] *Monorhaphis* spicules were determined to contain 9% water.[27] The existence of the

(20) Müller, W. E. G.; Rothenberger, M.; Boreiko, A.; Tremel, W.; Reiber, A.; Schröder, H. C. *Cell Tissue Res.* **2005**, *321*, 285–297.
(21) Schröder, H. C.; Boreiko, A.; Korzhev, M.; Tahir, M. N.; Tremel, W.; Eckert, C.; Ushijima, H.; Müller, I. M.; Müller, W. E. G. *J. Biol. Chem.* **2006**, *281*, 12001–12009.
(22) Müller, W. E. G.; Wang, X.; Kropf, K.; Ushijima, H.; Geurtsen, W.; Eckert, C.; Tahir, M. N.; Tremel, W.; Boreiko, A.; Schlossmacher, U.; Li, J.; Schröder, H. C. *J. Struct. Biol.* **2008**, *161*, 188–203.
(23) Michin, E. A. *Ergebn. Fortschr. Zool.* **1909**, *2*, 171–273.
(24) Compton, S.; Jones, C. *Anal. Biochem.* **1985**, *151*, 369–374.
(25) He, X. M.; Carter, D. C. *Nature* **1992**, *358*, 209–215.
(26) Müller, W. E. G.; Boreiko, A.; Schlossmacher, U.; Wang, X.; Tahir, M. N.; Tremel, W.; Brandt, D.; Kaandorp, J. A.; Schröder, H. C. *Biomaterials* **2007**, *28*, 4501–4511.
(27) Hyman, L. H. *The Invertebrates: Protozoa through Ctenophora*; McGraw-Hill: New York, 1940.
(28) Sandford, F. *Microsc. Res. Techn.* **2003**, *62*, 336–355.

interstitial water molecules between the biosilica nanospheres can also be visualized by SEM after heating the spicules to 450 °C.[29] Although the surfaces of natural spicules and lamellae are smooth and nonstructured (Figure 2C),[16] the lamellae in heated spicules obtain a distinct perforation composed of 1−2 μm large bubble craters (Figure 2G), which can be attributed to the evaporated interstitial water and to the organic material existing in the spicules.

The silicateins, members of the cathepsin L family,[8] were identified and isolated, and the gene was cloned − until now − only from demosponges.[9,10] Silicateins are distinguished from the proteinases by two characteristic sites, the catalytic triad [in the silicateins Ser-His-Asn, and in cathepsins Cys-His-Asn], and a conserved Ser cluster, which is located at the active site His, toward the N-terminal region. We have designed degenerate primers against the conserved regions of silicateins to isolate DNA sequences coding for silicatein from demosponges by polymerase chain reaction.[30] This technique was also successful for the first isolation of hexactinellid silicatein (shown here). At present, DNA from *Monorhaphis* could not be obtained from the ethanol-preserved tissue samples, which are older than 20 years. Therefore, longer segments of a cDNA or a gene coding for silicatein from *Monorhaphis* cannot be identified. Hence, we had to choose another hexactinellid sponge, *Crateromorpha meyeri* (Porifera, Hexactinellida, Lyssacinosida), for the isolation of the silicatein gene. The cDNA was isolated and that part, which had been previously shown to be sufficient for the preparation of recombinant and enzymatically active silicatein, was cloned (Figure 3).[11,31] The coding region, spanning the deduced protein from the beginning of the mature, enzymatically active protein to the end of the conserved region, including the third amino acid of the catalytic triad, was cloned; the sequence (cDNA) is deposited in the database (EMBL/GenBank; accession number AM920776). The deduced polypeptide possesses all characteristic sites known from the silicateins from demosponges;[9,11] for example, the typical catalytic triad amino acids [Ser_{22}-His_{161}-Asn_{181}], and the "conventional" Ser cluster [aa_{145} to aa_{158}] located adjacent to His, toward the N-terminus. Surprisingly, the hexactinellid silicatein protein comprises, in addition to this "conventional" Ser cluster, a second "hexactinellid-specific" Ser cluster that is located between aa_{169} and aa_{173} of the deduced *C. meyeri* polypeptide. Model prediction of the *C. meyeri* silicatein protein was performed using a comparative modeling process/procedure and complying with allowed regions of the Ramachandran areas.[32–34] The model prediction in Figure 4A unambiguously reveals that the "conventional" Ser cluster is spatially separated from the "hexactinellid-specific" Ser cluster; the position of the latter one (5 Ser residues) can be narrowed down to the outer loop of the exposed β-sheet (Figure 4A). In detail, $Ser_{169-171}$ are part of the β-sheet, whereas $Ser_{172-173}$ are located in the loop. Earlier considerations with diatoms led to the conclusion that the Ser and Thr residues in the cell walls of diatoms are involved in the interaction with the silicic acid residues.[35–37] The authors proposed a cross-link between a silicic acid molecule and the hydroxyl-containing side-chains of a serine−serine dipeptide from the silicalemma. Applying this standing model of an organic−inorganic interface to the potential function of the Ser cluster in the hexactinellid silicatein enzyme, we might suggest, in line with a previous report,[35–37] that the Ser dipeptides interact with the biosilica surfaces that pre-existed or were formed during the biosilicification reaction (Figure 4A). The five Ser residues (aa_{169} and aa_{173}) are supposed to interact with a polycondensated silica surface; an additional stabilization of this interaction is achieved by a further interaction with a Ser dipeptide (aa_{145} and aa_{146}), existing in the "conventional" Ser cluster. Those interactions might occur at pH values lower than 7, a pH which is reached within some sponge cells.[38] Phylogenetic analysis of the new *C. meyeri* silicatein was performed including related silicateins/cathepsins and *Arabidopsis thaliana* papain as a founding member of the cysteine protease family (Figure 3). The *C. meyeri* silicatein falls into the group of silicateins, forming with silicateins-ss the basis of the sponge silicateins. The cathepsins form a separate cluster with the *Aphrocallistes vastus* and the *C. meyeri* cathepsin-2 at the basis.

Inorganic Material of the Spicules: Quartz Glass. The hitherto described physical and chemical properties of the spicules showed that the composition of biosilica both in demosponges and hexactinellids is largely similar,[28] e.g., the density (2.1 g/cm^3), the transition temperature [T_g] (onset of T_g around 500 °C and first prominent exothermic event at 1000 °C), and the infrared spectra. Previously, the average chemical composition of the spicule was determined to be 85.2% for SiO_2, 12.3% water, and 2.5% other elements (mainly S, Al, K, Ca, and Na).[28,39] By Microprobe analysis, an at that time sensitive technique, *Monorhaphis* had been described to contain about 1% K_2O and 0.2% Na_2O.[39] Now, focusing on the hexactinellid *Monorhaphis*, the protein content was 4.6% [w/w] of the total weight of the spicules (this contribution), and 9% water;[27] the remaining material, mainly SiO_2 (86.4% [wt]), is inorganic components. The method of choice to determine trace elements in inorganic/organic fiber composite material quantitatively is the laser ablation-inductively coupled plasma-mass spectrometry (LA-ICPMS), because of the extreme sensitivity of the method (detection limits lower than ng g^{-1} range) and the possibility to measure a large array of elements simultaneously.[40] The unique and exceptional feature of the *Monorhaphis* giant

(29) Pisera, A. *Microsc. Res.Tech.* **2003**, *62*, 312–326.
(30) Müller, W. E. G.; Boreiko, A.; Wang, X.; Belikov, S. I.; Wiens, M.; Grebenjuk, V. A.; Schlossmacher, U.; Schröder, H. C. *Gene* **2007**, *395*, 62–71.
(31) Müller, W. E. G.; Krasko, A.; Le Pennec, G.; Steffen, R.; Ammar, M. S. A.; Wiens, M.; Müller, I. M.; Schröder, H. C. *Prog. Mol. Subcell. Biol.* **2003**, *33*, 195–222.
(32) Ramachandran, G. N.; Ramakrishnan, C.; Sasisekharan, V. *J. Mol. Biol.* **1963**, *7*, 95–99.
(33) Deane, C. M.; Blundell, T. L. *Protein Sci.* **2001**, *10*, 599–612.
(34) Robinson, P. N. A Java program for drawing Ramachandran plots. Available through the Internet via peter.robinson@charite.de (2007).
(35) Hecky, R. E.; Mopper, K.; Kilham, P.; Degens, E. T. *Mar. Biol.* **1973**, *19*, 323–331.
(36) Lobel, K. D.; West, J. K.; Hench, L. L. *Mar. Biol.* **1996**, *126*, 353–360.
(37) Lobel, K. D.; West, J. K.; Hench, L. L. *J. Mater. Sci. Lett.* **1996**, *15*, 648–650.
(38) Simpson, T. L. *The Cell Biology of Sponges*; Springer-Verlag: New York, 1984.

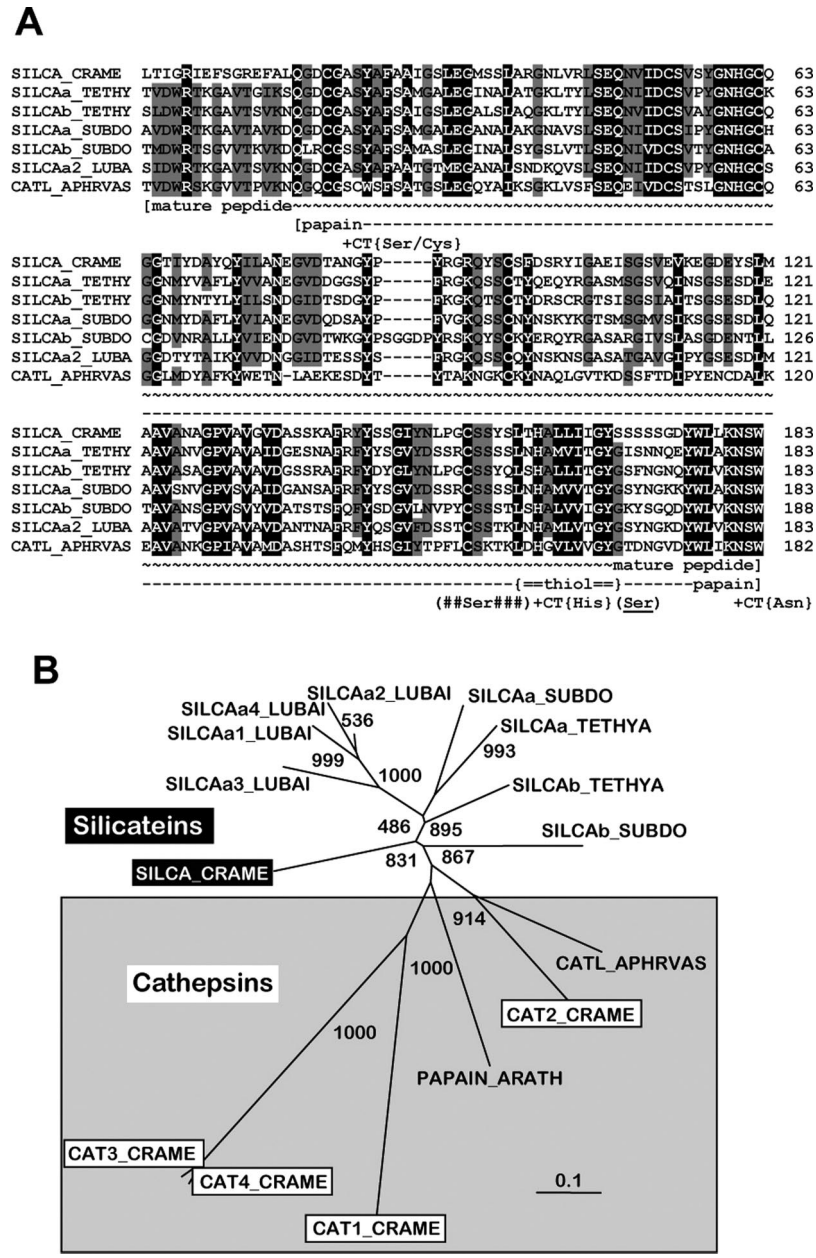

Figure 3. Silicatein protein, deduced from the *Crateromorpha meyeri* [Hexactinellida] cDNA (accession number AM904718). (A) The cDNA (*CMSILCA*) was isolated and the protein (SILCA_CRAME) was deduced. The hexactinellid silicatein was aligned with the two forms of silicatein both from the marine demosponges *Tethya aurantium* silicatein-α (SILCAa_TETYA; AAD23951) and silicatein-*β* (SILCA*β*_TETYA; AF098670) and from *Suberites domuncula* silicatein-α (SILCAa_SUBDO; AJ272013) and silicatein-*β* (SILCAb_SUBDO; AJ547635.1). In addition, one isoform of silicatein-α from the freshwater demosponges *Lubomirskia baicalensis* [α−2] (SILCAa2_LUBAI, AJ968945) and the cathepsin L sequence from hexactinellid *Aphrocallistes vastus* (CATL_APHRVAS, AJ968951) was used for this alignment. Residues conserved (similar or related with respect to their physicochemical properties) in all sequences are shown in white on black and those in at least four sequences in black on gray. The characteristic sites in the sequences are marked; the catalytic triad (CT) amino acids, Ser (+) in silicateins and Cys in cathepsin, as well as His (+) and Asn (+). The borders within the mature silicatein [mature peptide] of the following domains are given: the peptidase-C1 papain family cysteine protease domain (papain), and the thiol-protease-His signature (=thiol=). The "conventional" serine cluster (#Ser#), and the "*C. meyeri* specific" serine cluster (Ser) are marked. (B) From these six silicatein proteins, together with the hexactinellid cathepsin sequence from *A. vastus* and the three additional silicateins-α from the freshwater sponge *L. baicalensis* [α−1, α−3, and α−4] (SILCAa1_LUBAI, AJ872183; SILCAa3_LUBAI, AJ968946; SILCAa4_LUBAI, AJ968947) as well as the newly described cathepsin deduced proteins from *C. meyeri* (CAT1_CRAM, AM904719; CAT2_CRAM, AM904720; CAT3_CRAM, AM904721 and CAT4_CRAM, AM904722) the radial tree was constructed after the alignment. The numbers at the nodes are an indication of the level of confidence for the branches as determined by bootstrap analysis [1000 bootstrap replicates].

basal spicules is that a complete series of LA-ICPMS analyses can be performed on the same spicule within μm areas. We have chosen a 7 mm thick spicule (*Monorhaphis* from Qingdao [sample termed Q-B]) and determined 38 elements in individual 120 μm craters (depth of about 100 μm), from the axial canal toward the surface of the spicule (Figure 4B). We have chosen Si as the internal standard element, and accepted a SiO_2 content of 86% (wt) as

(39) Levi, C.; Barton, J. L.; Guillemet, C.; Le Bras, E.; Lehuede, P. *J. Mater. Sci. Lett.* **1989**, *8*, 337–339.

(40) Jochum, K. P.; Stoll, B.; Herwig, K.; Willbold, M. *J. Anal. Atom. Spectrom.* **2007**, *22*, 112–121.

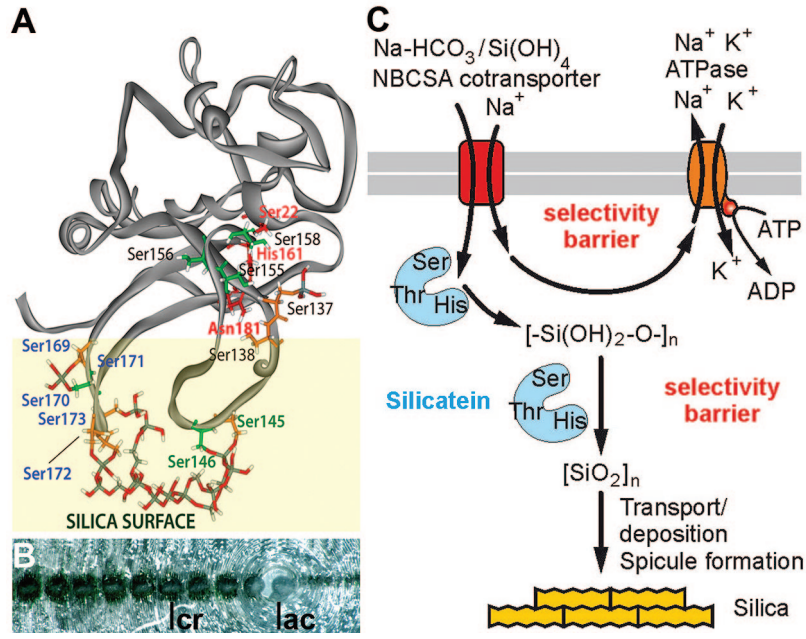

Figure 4. (A) Model of silicatein-α from the hexactinellid *C. meyeri*. The amino acids of the catalytic triad, in silicatein [Ser (aa_{22}), His (aa_{161}), and Asn (aa_{181})], are highlighted in red. In addition, the residues of the "hexactinellid specific" Ser cluster [$Ser_{169-173}$] are in blue; they are located at the large ss-sheet. It is proposed that these Ser residues interact with polycondensated silica surfaces within the lamellae of the spicules; an additional stabilization of this interaction is achieved by a further interaction with a Ser dipeptide [in green, Ser_{145} and Ser_{146}] of the "conventional" Ser cluster. (B) Cross section through a spicule showing the alignment of the craters (cr) produced during the LA-ICPMS analyses; the axial canal (ac) is marked. (C) Scheme outlining the two selectivity barriers that control the synthesis of the pure biosilica product. The Na^+-bicarbonate-/silicic acid- cotransporter mediates the uptake of silicate, allowing a strong selective enrichment of silicate in the cells and in the tissue of the sponges (first selectivity control). Na^+ is pumped out via the Na^+/K^+ ATPase pump under the consumption of ATP. The second selectivity control is on the level of silicatein, which will accept − substrate specifically − only silicate under formation of biosilica. Biosilica deposition is controlled by the organic scaffold, formed by silicatein and galectin.[16]

calculated above. Choosing an interspace of 150 μm, as much as 24 independent determinations across the same spicule could be performed (Table 1). The data reveal that the portion of Si in spicules accounts for 4.0×10^5 μg/g. It is of prime interest that the contribution of the trace elements to the total inorganic components in the spicules is less than 0.005-fold with respect to Si (Figure 5A). This implies that the quality of biosilica in the spicules is in the range of quartz grade,[41] with respect to the low concentrations of the elements other than silicon and oxygen. These trace elements are split as follows; among the monovalent counterions Na^+ contributes to 86% (wt) [0.21% (wt) with respect to total inorganic material in the biosilica] and among the divalent ions Ca^{2+} to 12% (wt) [0.03% (wt)] (Figure 5B). All other 35 remaining elements contribute with <2% (wt) only unimportantly to the inorganic composition of the trace elements in biosilica (see the section of the pie diagram in Figure 5B). We have performed the same analyses with five different spicules, from different regions, and found no considerable differences in the chemical composition (to be published). The impact of this finding becomes even more meaningful in comparison with the element composition of seawater. Referring to natural seawater Na and Cl are dominant with 32.4% and 58.5% [solid material], respectively.[42] Mg contributes 3.9%, Ca 1.2%, and Si only 0.006% (Figure 5C). The present day seawater contains very little Si,[43,44] in contrast to aqueous environment in the geological time when the sponges evolved in the late Proterozoic, approximately 500−800 million years ago.[45] In that era, the marine environment was rich in silicon and very suitable for the earliest metazoans [Urmetazoa], the Porifera, to develop a siliceous skeleton. Amazingly, the experimental data shown here demonstrate that the sponges produce almost pure biosilica in an aqueous environment, which contains only trace levels of Si.[42,46] The other very significant outcome of our LA-ICPMS analyses was the finding that the distribution of the elements across the axis of the spicule does not change considerably (Table 1). The graph shows (Figure 5D) that the dominant elements, the alkali metals Na and Rb as well as the alkaline earth metals Mg, Ca, and Sr, do not change markedly from the axial canal to the surface of the spicule.

The data of this contribution show that Hexactinellida have developed the fascinating ability to produce enzymatically amorphous quartz glass as the material to construct their biosilica skeleton, and perhaps also chitin[13] and collagen.[12] In contrast, the industrial fabrication of this ultrahard (almost) pure silicon dioxide material requires processes involving

(41) Foissy, A.; Persello, J. Surface group ionization on silicas. In *The Surface Properties of Silicas*' Legrand, A. P., Ed.; John Wiley: Chichester, U.K., 1998; pp 365−414.
(42) Kennish, M. J., Ed. *Practical Handbook of Marine Science*; CRC Press: Boca Raton, FL, 1994.
(43) Maldonado, M.; Carmona, M. C.; Uriz, M. J.; Cruzado, A. *Nature* **1999**, *401*, 785–788.
(44) Maldonado, M.; Carmona, M. C.; Velásquez, Z.; Puig, M. A.; Cruzado, A. *Limnol. Oceanogr.* **2005**, *50*, 799–809.
(45) Müller, W. E. G.; Li, J.; Schröder, H. C.; Qiao, L.; Wang, X. *Biogeosciences* **2007**, *4*, 219–232.
(46) Miserez, A.,; Weaver, J. C.; Thurner, P. J.; Aizenberg, J.; Dauphin, Y.; Fratzl, P.; Morse, D. E.; Zok, F. W. *Adv. Funct. Mater.* **2008**, *18*, 1241–1248.

Table 1. Concentrations (μg/g) in Different Spots (spot size = 120 μm) of Sample Q-B (from axial canal to rim)[a]

	Q-B-1	Q-B-2	Q-B-3	Q-B-4	Q-B-5	Q-B-6	Q-B-7	Q-B-8	Q-B-9	Q-B-10	Q-B-11	Q-B-12	Q-B-13	Q-B-14	Q-B-15	Q-B-16	Q-B-17	Q-B-18	Q-B-19	Q-B-20	Q-B-21	Q-B-22	Q-B-23	Q-B-24	Mean
Na	1967	1735	2325	1430	1543	1360	1373	1431	1467	1385	1290	1445	1442	2225	1370	1560	1351	1302	1891	1380	1460	1428	1877	1997	1549
Mg	41.7	11.1	14.5	12.6	20.4	16.4	15.8	15.0	20.2	26.9	30.7	55.5	56.9	46.0	68.2	32.1	29.5	21.4	21.7	31.3	28.1	24.5	44.7	60.8	29.2
Ca	895	387	237	183	162	146	189	97	165	138	129	172	129	211	237	229	271	156	222	205	257	215	442	267	208
Ti	4.18	1.17		0.34	0.37	3.02	1.90		10.63	4.03	2.57	0.79	4.23	0.06	1.28	1.48	0.29	4.39	0.49	2.81		0.81	2.35	18.16	2.26
Co	0.282	0.106	0.130	0.172	0.081	0.126	0.114	0.107			0.012	0.095	0.022	0.149	0.158	0.048	0.219	0.018	0.110	0.169	0.146	0.013		0.209	0.105
Ni	4.87	0.50	0.58	0.09		2.51	1.52	0.78	1.00	1.47	1.95	1.13	1.95	2.88			1.19			3.19				0.49	1.48
Cu	3.02	0.46	0.84	0.89	6.42	11.54	7.02	13.94	6.36	3.17	1.78	0.97	2.69	0.79	2.43	0.51	0.40	0.65	2.48	9.49	3.00	1.68	0.86	1.56	3.56
Zn	6.15	3.25	1.19	3.89	1.95	1.69	2.60	1.83	3.54	2.81	3.18	22.64	4.53	8.76	1.68	4.09	4.03	1.70	4.85	4.25	2.73	1.99	5.49	9.01	4.21
Ge	0.33	0.22	0.25	0.25	0.24	0.27	0.19	0.25	0.35	0.26	0.22	0.05	0.07	0.24	0.18	0.22	0.19	0.22	0.31	0.24	0.23	0.14	0.31	0.20	0.22
Rb	7.68	7.32	7.86	7.91	8.50	8.79	8.84	8.60	9.34	9.62	9.30	10.06	10.11	9.90	9.85	10.14	10.21	9.52	10.22	10.09	10.52	10.23	10.43	11.28	9.43
Sr	0.69	0.73	0.34	0.36	0.30	0.24	0.29	0.27	0.49	0.37	0.65	0.41	0.69	1.20	0.56	0.59	0.59	0.60	0.57	0.95	0.88	0.68	1.24	1.58	0.59
Y	0.223	0.041	0.050	0.053	0.099	0.051	0.051	0.048	0.087	0.066	0.055	0.051	0.100	0.060	0.070	0.102	0.076	0.089	0.075	0.105	0.093	0.070	0.096	0.157	0.072
Zr	0.236	0.052	0.062	0.038	0.037	0.042	0.044	0.026	0.066	0.049	0.069	0.061	0.057	0.096	0.086	0.081	0.059	0.071	0.047	0.069	0.123	0.066	0.122	0.162	0.065
Nb	0.269	0.203	0.053	0.048	0.022	0.019	0.037	0.121	0.034	0.065	0.057	0.037	0.052	0.039	0.071	0.038	0.054	0.015	0.011	0.012	0.027	0.049	0.072	0.104	0.052
Mo	0.299	0.176	0.138	0.165	0.062	0.111		0.081	0.031	0.102	0.057	0.138	0.013	0.034	0.073	0.095	0.052	0.013	0.077	0.038		0.086	0.055	0.147	0.080
Rh	0.009		0.001	0.007	0.003		0.002	0.007			0.006		0.001	0.003		0.003		0.001	0.002	0.001	0.003		0.000		0.003
Pd	0.059	0.089	0.060	0.051	0.030	0.060	0.081	0.041	0.064	0.047	0.068	0.043	0.050	0.107	0.038	0.078	0.050	0.109		0.050		0.072	0.040	0.078	0.061
Ag	0.085	0.070	0.038	0.004	0.003	0.022		0.040	0.029	0.001	0.004	0.041	0.021	0.013	0.014	0.033	0.006	0.010	0.021	0.014	0.007	0.021	0.045	0.017	0.022
Cd	0.443	0.342	0.155	0.032	0.435	0.402	0.242	0.261	0.696	0.212	0.129		0.214	0.204	0.245		0.141	0.001	0.170	0.067	0.085	0.364	0.134	0.237	0.227
In	0.370	0.360	0.109	0.082	0.055	0.013	0.057	0.034	0.034	0.044	0.025	0.048	0.070	0.075	0.059	0.031	0.003	0.017	0.071	0.009	0.014	0.034	0.095	0.221	0.061
Sn	0.782	0.679	0.591	0.540	0.549	0.512	0.595	0.465	0.485	0.539	0.502	0.552	0.652	0.546	0.558	0.638	0.592	0.565	0.513	0.529	0.559	0.592	0.545	1.434	0.559
Ba	0.426	0.201	0.074	0.179	0.193	0.293	0.196	0.356	0.761	0.456	0.416	0.279	0.388	0.438	0.715	0.303	5.375	0.788	0.507	0.543	0.286	0.222	0.264	0.526	0.601
La	0.183	0.071	0.139	0.056	0.023	0.077	0.072	0.034	0.079	0.053	0.046	0.044	0.057	0.051	0.051	0.074	0.037	0.052	0.057	0.070	0.100	0.051	0.089	0.115	0.063
Ce	0.413	0.310	0.120	0.097	0.147	0.115	0.095	0.100	0.204	0.062	0.099	0.088	0.116	0.091	0.078	0.091	0.116	0.088	0.135	0.158	0.143	0.113	0.113	0.282	0.122
Nd	0.224	0.121	0.052	0.062	0.108	0.074	0.052	0.031	0.055	0.052	0.046	0.067	0.036	0.055	0.071	0.056	0.079	0.046	0.052	0.078	0.061	0.076	0.088	0.091	0.064
Dy	0.097	0.074	0.073	0.027	0.079	0.062	0.016	0.014	0.016	0.026	0.021	0.032	0.029	0.019	0.008	0.012	0.024	0.014	0.008	0.025	0.071	0.014	0.027	0.068	0.031
Er	0.063	0.050	0.065	0.011	0.034	0.010	0.020	0.019	0.032	0.031	0.056	0.024	0.028	0.017	0.055	0.010	0.012	0.019	0.014	0.048	0.020	0.019	0.032	0.028	0.028
Yb	0.110	0.094	0.034	0.019	0.035	0.021	0.037	0.030	0.036	0.058	0.028	0.031	0.043	0.031	0.033	0.024	0.047	0.044	0.063	0.013	0.040	0.043	0.070	0.049	0.040
Hf	0.091	0.038	0.072		0.032	0.020	0.006	0.018	0.022		0.010	0.014	0.014	0.000	0.005	0.003	0.020	0.007	0.031	0.020	0.006	0.022	0.029	0.018	0.019
Ta	0.198	0.081	0.060	0.047	0.030	0.058	0.037	0.045	0.098	0.063	0.043	0.039	0.062	0.082	0.096	0.052	0.051	0.039	0.051	0.073	0.077	0.054	0.088	0.151	0.060
W	0.367	0.233	0.270	0.188	0.084	0.100	0.265	0.148	0.035		0.241	0.149	0.094	0.073	0.261	0.267	0.312	0.042	0.089	0.017	0.117	0.712	0.099	0.000	0.181
Pt	0.011	0.002	0.008		0.001			0.014	0.009		0.003	0.006	0.003	0.011	0.002	0.013	0.004	0.006	0.007		0.007		0.003		0.006
Tl	0.054	0.024	0.007	0.010	0.005	0.025	0.010		0.010		0.007	0.009	0.007	0.004	0.034	0.023	0.007	0.012	0.007		0.019	0.033	0.011	0.002	0.014
Pb	0.349	0.161	0.103	0.203	0.049	0.110	0.046	0.112	0.117	0.059	0.092	1.355	0.405	1.304	0.431	0.410	0.195	0.128	0.159	0.209	0.145	0.155	1.104	1.779	0.320
Bi	0.179	0.076	0.048	0.015	0.061	0.024	0.023	0.117	0.081		0.022	0.037	0.004	0.026	0.028	0.018	0.022	0.017	0.125	0.038	0.042	0.049	0.034	0.040	0.043
Th	0.126	0.073	0.038	0.044	0.047	0.044	0.020	0.041	0.037	0.023	0.038	0.047	0.034	0.028	0.031	0.042	0.019	0.034	0.027	0.025	0.025	0.049	0.056	0.061	0.037
U	0.516	0.312	0.106	0.159	0.107	0.065	0.032	0.106	0.112	0.023	0.074	0.062	0.102	0.029	0.064	0.109	0.040	0.011	0.056	0.126	0.049	0.065	0.163	0.056	0.090

[a] Distances between spots are 150 μm. Mean values do not contain the data from the axial canal and the rim.

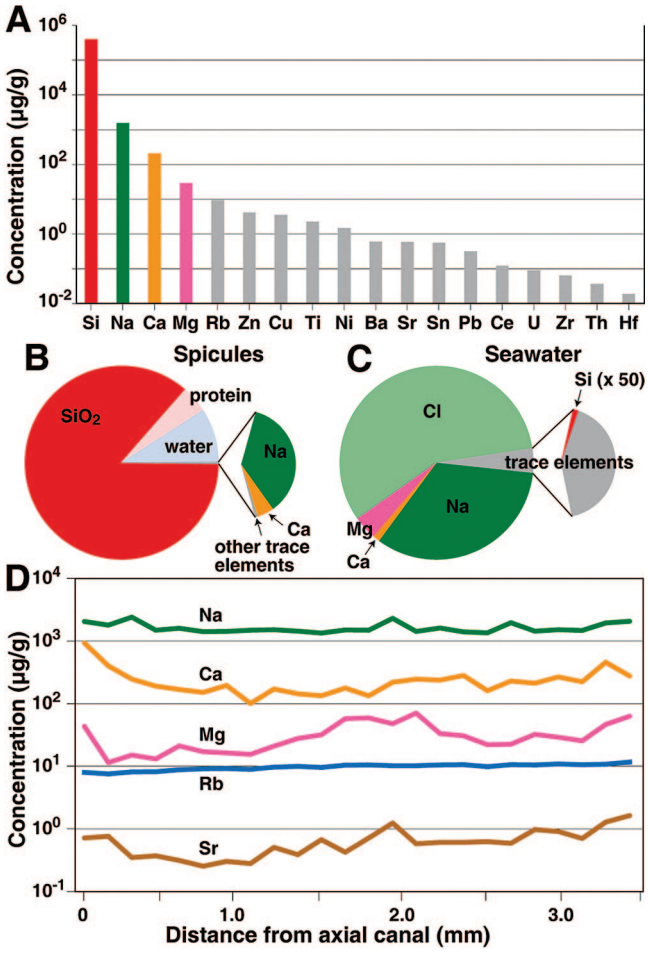

Figure 5. LA-ICPMS analyses. (A) Concentrations (μg/g) within the *Monorhaphis* spicule Q-B; the elements are arranged according to their abundance. Please note the logarithmic scale of the abscissa. (B) Pie diagram, showing the abundance of SiO_2, protein, and water, in comparison to the low portion of trace elements (sector part), including Na- and Ca-oxides, and further trace components. (C) A comparative diagram showing the distribution of these elements in seawater; there, Si exists as a trace element, as seen in the sector piece, whereas Cl, Na, Mg, and Ca are abundant. (D) Distribution of selected alkali metals (Na and Rb) as well as alkaline earth metals (Mg, Ca, and Sr) along the cross axis of a spicule. The distance from the axial canal to the surface of the spicule where the 24 individual element analyses were performed is given in millimeters. The element concentrations have been determined in the 120 μm areas.

aggressive chemicals [3N HCl or 5N H_2SO_4] and extreme temperatures [above 1800 °C]. Excitingly, prior to the discovery of "enzymic glass" in sponges, it was unthinkable that such amorphous glasses could be produced at temperatures below 30 °C. Among the siliceous sponges the first class of Porifera, the Hexactinellida, comprises one species [*Monorhaphis chuni*] that builds its bodies around one gigantic spicule [giant basal spicule], reaching heights of 3 m.[18] Because of their enormous size, the giant basal spicules from *Monorhaphis* provide the exceptional opportunity to study the distribution of elements even across one spicule section. Similar experiments should follow with spicules from the taxa Hyalonema, or Farrea.

Conclusions

In conclusion, our data show unexpectedly and fascinatingly that the giant basal spicule(s) from the hexactinellid *Monorhaphis* are composed of almost pure SiO_2 (>99.5%). Considering the fact that the present day oceans are poor in Si and rich in Na this extreme disproportion asks for a biochemical explanation, which we can give here. The extreme enrichment of Si in the cells/body of the sponges is the result of two "selectivity barriers/fractionation sites", (i) an energy dependent pumping system which we described earlier[47] and (ii) the substrate specificity of the enzyme silicatein. We could demonstrate that in membranes of sponge cells a Na^+/HCO_3^- $[Si(OH)_4]$ cotransporter exists that pumps $Si(OH)_4$ into the cells probably on expense of energy, very likely generated by the arginine kinase.[47,48] The pump, which overcomes the membrane gate for silicic acid, is certainly substrate/ion-specific and hence specifically concentrates silicon/silicate (Figure 4C). Second, because (intracellularly) the synthesis of biosilica of the spicules from hexactinellids is mediated by silicatein, this enzyme will certainly catalyze substrate specifically.[11] On the basis of these two "selectivity barriers", the formation of the pure silica glass product becomes mechanistically obvious (Figure 4C).

Quartz glasses of the quality of the material in spicules, because of their exceptional optical and chemical properties, are ideally suited for the fabrication of complex designs in semiconductor lithography and three-dimensional microscale processing techniques.[49,50] At present, the application of quartz glasses is limited because of the lack of technologies to manufacture quartz glass structures by chemical methods at micro- and nanoscale, and especially at organo-compatible temperatures. One major progress can be expected in this field from the present report, which provides the reaction mechanism by which nature − sponges − accomplishes the formation of biosilica of quartz glass grade at physiological temperature and pH conditions. This mechanism, driven by silicatein, may surely be applicable for biotechnological purposes in the nearest future. This optimistic view is strongly supported by the fact that the crucial enzyme, silicatein, is available in an active recombinant form.[11] The biotechnological application of this process will allow the synthesis of pure quartz glass useful for the fabrication of semiconductors (at microscale) on organic matrices. Furthermore, silicatein has the potential to synthesize titania- and zirconia-doped silica glasses or fibers that are known to show low thermal expansions and low variations in thermal expansion. The likely proof of concept for the latter application has been given earlier.[48]

Experimental Section

The relevant methods have been described earlier.[8,10,16,20]

Spicules (giant basal spicules). Spicules from the hexactinellids *Monorhaphis chuni/M. intermedia* have been provided by the Marine Biological Museum of Chinese Academy of Sciences in

(47) Schröder, H. C.; Perović-Ottstadt, S.; Rothenberger, M.; Wiens, M.; Schwertner, H.; Batel, R.; Korzhev, M.; Müller, I. M.; Müller, W. E. G. *Biochem. J.* **2004**, *381*, 665–673.
(48) Tahir, M. N.; Théato, P.; Müller, W. E. G.; Schröder, H. C.; Boreiko, A.; Faiss, S.; Janshoff, A.; Huth, J.; Tremel, W. *Chem. Commun.* **2005**, *44*, 5533–5535.
(49) Xia, Y.; Whitesides, G. M. *Annu. Rev. Mater. Sci.* **1998**, *28*, 153–184.
(50) Lee, L. P.; Szema, R. *Science* **2005**, *310*, 1148–1150.

the Institute of Oceanography (Qingdao [China]; Chinese Academy of Sciences) and used for the chemical and biological studies. The spicules were cleaned from remaining tissue in sulfuric/nitric acid, and were finally washed with distilled water, as described.[16] Protein was isolated from the spicules by grinding the material with a Tris-buffered saline buffer (pH 7.5, 1 mM EDTA, 1% Nonidet-P40), supplemented with 4 M urea.[10] The protein composite component was determined as described,[21] using the Roti-Quant reagent (Roth, Karlsruhe; Germany).[24] *Crateromorpha meyeri* was dredged in the Sagami Bay, Japan; animals were immediately transferred into ethanol until use for the molecular biological studies. SEM analyses were performed with broken spicules or cross sections. For $NaDodSO_4$-PAGE, 10% polyacrylamide gels containing 0.1% sodium dodecyl sulfate have been used.[20] For Western blot analysis, the polyclonal antibodies, prepared against the *S. domuncula* silicatein were applied.[16] Spicule dissolution was achieved with hydrofluoric acid.[8]

Cloning of Silicatein. The cloning strategy for the identification and isolation of the cDNA from the hexactinellid sponge *C. meyeri* was described before.[30] First, a *C. meyeri* cDNA library was prepared by reverse transcribing purified mRNA; dscDNA was ligated to an attB1 adapter and used to perform a recombination with the pDONR222 vector (Invitrogen, Karlsruhe, Germany), catalyzed by BP clonase. The cDNA library was obtained by transformation of DH10B T1 phage resistant *Escherichia coli* cells. Sequences were analyzed using computer programs BLAST (http://www.ncbi.nlm.nih.gov/blast/blast.cgi) and FASTA (http://www.ncbi.nlm.nih.gov/BLAST/fasta.html). Modeling of the *C. meyeri* silicatein was approached by selecting the most similar sequence, human cathepsin K (accession number CAI12795), and using the improved alignment algorithm for matching biological sequences (MODELER application). After the energy-minimized model was calculated, the predicted stereochemical configuration was validated.[51,52]

Trace Elements. Analyses were performed LA-ICPMS combining a sector-field ThermoFinnigan Element 2 mass spectrometer and a New Wave UP 213 laser ablation system.[40] Spot sizes used were 120 μm. The internal standard element was Si; a SiO_2 content of 86% [wt] was taken, based on the data given here. Calibration was performed with NIST SRM 612 glass, using the values published in the GeoReM database (http://georem.mpch-mainz.gwdg.de). The detection limits range between 0.3 and 10 ng/g. Uncertainties of the analytical data vary between 5 and 15%, depending on the concentration.

For the alignment and the construction of the phylogenetic tree the computer programs BLAST (2003; http://www.ncbi.nlm.nih.gov/blast/blast.cgi) and FASTA algorithms (2003; http://www.ncbi.nlm.nih.gov/BLAST/fasta.html) have been used. Multiple alignments were performed with CLUSTAL W version 1.6.[53] Phylogenetic trees were constructed on the basis of protein sequence alignments by neighbor-joining, as implemented in the "Neighbor" program from the PHYLIP package.[54] The distance matrices were calculated using the Dayhoff PAM matrix model as described.[55] The degree of support for internal branches was further assessed by bootstrapping.[54] The graphic presentations were prepared with GeneDoc.[56]

Acknowledgment. This work was supported by grants from the Bundesministerium für Bildung and Forschung Germany (project "Center of Excellence *BIOTEC*marin"), the International Human Frontier Science and the Basic Scientific Research Program in China (Grant 200607CSJ-05). We thank Mr. G. Glasser (Research group "Surface Chemistry" Prof. H. J. Butt, and Dr. I. Lieberwirth, Max Planck Institute for Polymer Research, Mainz) for excellent assistance in electron microscopic analysis. Additionally, we thank Drs. A. Boreiko, U. Schlossmacher, K. Kropf, D. Brandt, and Prof. H.C. Schröder (Institut für Physiologische Chemie, Universität Mainz) for significant contributions. We thank Dr. I. Domart-Coulon (Museum National d'Histoire Naturelle, Paris), Dr. D. Janussen (Department of Marine Evertebrates I, Research Institute and Natural Museum Senckenberg, Frankfurt/Main) and Marine Biological Museum of Chinese Academy of Sciences (Qingdao) for providing sponge samples.

CM800734Q

(51) Sali, A.; Blundell, T. L. *J. Mol. Biol.* **1993**, *234*, 779–815.
(52) Vriend, G.; What, I. F. *J. Mol. Graph.* **1990**, *8*, 52–56.
(53) Thompson, J. D.; Higgins, D. G.; Gibson, T. J. *Nucleic Acids Res.* **1994**, *22*, 4673.
(54) Felsenstein, J. *PHYLIP*, version 3.5; University of Washington: Seattle, WA, 1993.
(55) Dayhoff, M. O.; Schwartz, R. M.; Orcutt, B. C. In *Atlas of Protein Sequence and Structure*; Dayhoff, M. O., Ed.; Nature Biomedical Research Foundation: Washington, D.C., 1978; pp 345−352.
(56) Nicholas, K. B.; Nicholas, H. B. cris.com/~ketchup/genedoc.shtml; distributed by the author.